NASA-CR-200234

NAS5-1463

1N-90-CR
8475
P 35

Dust in the Small Magellanic Cloud: I. Interstellar Polarization and Extinction Data

A. M. Magalhães[1,2,3,4] and C. V. Rodrigues[5]
Instituto Astronômico e Geofísico - USP
Caixa Postal 9638, São Paulo - SP 01065-970, Brazil
e-mail: mario@argus.iagusp.usp.br, claudia@das.inpe.br

G. V. Coyne, S. J.
Vatican Observatory
V-00120 Vatican City State, Rome, Italy
e-mail: specola_vat@astrom.dnet.nasa.gov

and

V. Piirola
Tuorla Observatory - University of Turku
SF-21500 Piikkiö, Finland
e-mail: piirola@sara.cc.utu.fi

ABSTRACT

The typical extinction curve for the Small Magellanic Cloud (SMC), in contrast to that for the Galaxy, has no bump at 2175 Å and has a steeper rise into the far ultraviolet. For the Galaxy the interpretation of the extinction and, therefore, the dust content of the interstellar medium has been greatly assisted by measurements of the wavelength dependence of the polarization. For the SMC no such measurements existed. Therefore, to further elucidate the dust properties in the SMC we have for the first time measured linear polarization with five colors in the optical region of the spectrum for a sample of reddened stars. For two of these stars, for which there were no existing UV spectrophotometric measurements, but for which we measured a relatively large polarization, we have also obtained data from the International

---

[1]Guest observer at IUE

[2]Visiting Astronomer, Cerro Tololo Inter-American Observatory. CTIO is operated by AURA, Inc. under contract to the National Science Foundation

[3]Visiting Astronomer, Complejo Astronomico El Leoncito, San Juan, Argentina

[4]Visiting Astronomer, European Southern Observatory, La Silla, Chile

[5]now at Inst. Nacional de Pesquisas Espaciais-INPE, Divisão de Astrofísica-DAS, Caixa Postal 515, São José dos Campos - SP 12201-970, Brazil

Ultraviolet Explorer (IUE) in order to study the extinction. We also attempt to correlate the SMC extinction and polarization data.

The main results are: (1) the wavelength of maximum polarization, λ_{max}, in the SMC is typically smaller than that in the Galaxy; (2) however, AZV 456, which shows the UV extinction bump, has a λ_{max} typical of that in the Galaxy, but its polarization curve is narrower and its bump is shifted to shorter wavelengths as compared to the Galaxy; (3) from an analysis of both the extinction and polarization data it appears that the SMC has typically smaller grains than those in the Galaxy. The absence of the extinction bump in the SMC has generally been thought to imply a lower carbon abundance in the SMC compared to the Galaxy. We interpret our results to mean that the size distribution of the interstellar grains, and not only the carbon abundance, is different in the SMC as compared to the Galaxy. In Paper II we present dust model fits to these observations.

Subject headings: ISM: dust, extinction - polarization - ultraviolet: interstellar - galaxies: Magellanic Clouds

1. Introduction

The interstellar medium (ISM) in galaxies is indicative of their evolutionary state and of their stellar populations. For instance, the Galaxy contains four times more heavy elements than the Large Magellanic Cloud (LMC) and ten times more than the Small Magellanic Cloud (SMC) (Wheeler, Sneden & Truran 1989). The dust content of the ISM in the LMC (Koorneef 1982; Fitzpatrick 1985a) and SMC (Bouchet et al 1985; Fitzpatrick 1985b) is less than in the Galaxy and the dust is qualitatively different. In particular, the SMC has a steeper far ultraviolet (FUV) extinction curve (Prévot et al. 1984); it typically has no ultraviolet (UV) extinction bump. The SMC has also a weak infrared (IR) emission at 12 μm and an intensity ratio 60μm$/100\mu$m larger than that in the Galaxy (Lequeux 1989). This would appear to indicate that star formation and evolution has proceeded at a faster rate in the Galaxy than in the LMC or SMC and/or that dust grains have formed there differently in a different environment. In fact, there is some indication that the efficiency of grain formation in the LMC and SMC may be slightly lower, albeit similar, compared to that in the Galaxy (Clayton and Martin 1985). Also, from data on M31, it is suggested that the abundance of small grains may be related to star formation rates (Xu & Helou 1994).

For these reasons and because of its proximity the SMC is an important environment in which to study dust grains. Dust may cause several observable effects by which its nature may be studied: it attenuates, reddens, scatters and polarizes starlight; it absorbs and reemits radiation; it may bring about a depletion of the gas content of the ISM and may serve as a catalyst for the formation of molecules in the ISM. In the case of the SMC, the higher FUV radiation field together with the lower dust content produces an increased photodissociation of molecules that affects the properties of molecular clouds (Lequeux et al 1994). The SMC is thus an excellent laboratory to study dust in an environment quite distinct from that of the Galaxy, while at the same time allowing us to test dust models which have been proposed. We concentrate our study on the reddening and the polarization due to dust in the SMC.

It has been known for some time from IUE observations that the UV and FUV extinction relative to the visual and the IR is much larger in both the LMC (Nandy et al 1981; Koorneef and Code 1981; Fitzpatrick 1985a, 1986) and in the SMC (Prévot et al 1984) than it is in the Galaxy and the effect is larger for the SMC than it is for the LMC. The SMC is also noteworthy for the lack of the extinction bump at 2175 Å (see review by Fitzpatrick 1989). Interstellar polarization in connection with extinction in the LMC context has been studied by Clayton, Martin & Thomson (1983), Clayton & Martin (1985) and Clayton et al. (1996).

Classical models for fitting the wavelength dependence of the extinction by dust grains in the ISM of galaxies generally take into account the chemical composition of the grains and their size distribution. For grains in the Galaxy it is known that the wavelength at which the polarization is maximum is related to the grain size (Coyne, Gehrels and Serkowski 1974). It would, therefore, be very useful to have this information for the SMC. No wavelength dependent polarization measurements have been yet published on the SMC. In this paper we present the first such observations and analyze them in light of the extinction for which we also report a few new IUE observations. In Paper II (Rodrigues, Magalhães and Coyne 1995) we present detailed model fits to these observations.

2. Data

2.1. Polarization Data

2.1.1. Observations

Polarimetric observations have been obtained during several observing runs at various observatories and with various polarimeters. The observing runs were: 1983 with the MINIPOL polarimeter (Frecker and Serkowski 1976) on the 1.5 meter telescope at the Cerro Tololo Interamerican Observatory (CTIO); 1987 with the PISCO polarimeter (Stahl et al. 1986) on the 2.2. meter telescope of the European Southern Observatory (ESO); and 1986, October 1988, November 1988 and 1989 with the VATPOL polarimeter (Magalhães, Benedetti and Roland 1984) on the 2.15 meter telescope at the Complejo Astronomico El Leoncito (CASLEO). About seventy percent of the observations were made at CASLEO.

VATPOL and MINIPOL provide on-line data reduction after each integration and/or after a series of integrations (the integration time can be freely selected). This data reduction consists of a least squares fit to a double cosine curve of the counts from two photomultiplier tubes obtained as a function of the position of a rotating half-wave plate. The standard deviation of the counts from the double cosine curve is also calculated and we take this as the measurement error, which is typically consistent with the photon-noise error (Magalhães et al. 1984). The data from PISCO were obtained in FITS format and we wrote a special microcomputer program to calculate the polarization from the star and sky counts in a way similar to that just described.

All data have been corrected for instrumental effects and have been standardized. Unpolarized standard stars were measured to obtain corrections for instrumental polarization. Nightly measurements were made on highly polarized standard stars and also with a Glan prism in the beam in order to obtain the polarizing efficiencies and to standardize the polarization position angles to the equatorial system. The polarizing efficiencies were typically 98 to 99 % for VATPOL and MINIPOL. For the measurements with PISCO the efficiencies were provided to us by Hugo Schwarz of ESO. Repeated runs at CASLEO showed all corrections measured there to be stable. Corrections for bias in the linear polarization, which depend on the ratio of the error to the percentage polarization (Clarke and Stewart 1986), were also applied. We note, however, that all calculations were made using the Stokes parameters.

We combine the results from the three instrumental systems in the following way. For each star we calculate first the weighted average of the measurements made with each filter in each of the instrumental systems. We then determine the weighted mean of those averages. The results, both observed and corrected for foreground polarization (see sec. 2.1.2) are given in Table 1, where the respective columns are: (1) star number from Azzopardi & Vigneau (1982, AZV82); (2) star number from Sanduleak (1968, 1969); (3)-(5): the observed polarization, equal to the weighted mean polarization over the averages obtained from each observing run, the standard deviation of the mean and the polarization position angle in the equatorial system, respectively; (6)-(8): same as colums (3)-(5) but for the foreground corrected polarization; (9) the effective wavelength (averaged over the values for each observing run, by weighting with the mean polarization errors). The foreground-corrected polarization measurements are plotted in Fig. 1.

The targets reported in Table 1 have been selected for multifilter polarimetry from our on-going program to map the magnetic field structure of the SMC (Magalhães et al. 1990). The sample was built from the AZV82 catalog, avoiding stars with emission line spectrum. This survey is presently being conducted with CCD imaging polarimetry (Magalhães et al. 1996) and the results will be reported elsewhere.

2.1.2. Foreground Polarization Corrections

It is necessary to correct the measured polarizations by subtracting the polarization foreground to the SMC due mainly to dust in the Galaxy. It is expected that these corrections are important, since the interstellar reddening intrinsic to the SMC is small. We have selected published, unfiltered polarization data (Mathewson and Ford 1970; Schmidt 1976) on about 40 stars farther than 400 pc from the Sun in the direction of the stars measured in the SMC. McNamara and Feltz (1980) have shown that most of the foreground extinction to the SMC occurs within 400 pc from the Sun. Also by this selection we include most of the dust in the galactic plane for which the scale height is 120 pc (Burton et al. 1986).

As a check on this procedure, we have also estimated the foreground polarization in two additional ways. The first of these was to average the polarization data of our survey sample (Magalhães et al. 1990, Rodrigues 1992) for stars in the SMC which showed an observed polarization equal to or less than 0.4%. We have also averaged, again using data from our survey, polarization data for SMC stars which had an estimated color excess less than 0.09^{mag}. This upper limit for the foreground reddening towards the SMC is suggested by Schwering (1988); McNamara and Feltz (1980) and Bessel (1991) have suggested lower values (0.02^{mag} and $0.04^{mag} - 0.06^{mag}$, respectively). We have estimated the color excess for the SMC stars in our sample using the intrinsic colors from Fitzgerald (1970) and Brunet (1975). Both of these methods gave results that were entirely consistent with the estimates from the Galatic foreground objects (Table 2) described in the previous paragraph and which we used for correcting the SMC data.

Table 2 gives the adopted corrections for the foreground polarization towards the various regions in the SMC defined by Schmidt (1976). Our program stars are located as follows: region I, AZV 20, 126, 221; region II, AZV 211, 215, 398; region III, AZV 456.

The estimated values for the foreground polarization were taken as valid for the V filter. We used the Serkowski law, with λ_{max}=0.55μm, to estimate the contribution in the other filters. The corrected polarization values carry the increase in uncertainty arising from this correction. These are the values in Table 1. We tested the influence of changes in λ_{max} on the above estimates and on the resulting corrected data and found them to be insignificant.

2.2. UV spectroscopic data

Our UV sample consisted of three reddened stars, AZV 20, AZV 126 and AZV 211, and comparison stars necessary to obtain the extinction curves (see sec. 2.2.2). AZV 211 was our primary target because it had shown a well determined polarization curve with a small λ_{max} (Fig. 1 and Table 4). We have included in our reduction the data already published on AZV 398 (Prévot et al. 1984) and on AZV 456 (Lequeux et al. 1984) in order to test our procedure and to give homogeneity to the sample studied in the following sections. The relevant data on the reddened stars and on the comparison stars are given in Tables 3a and 3b respectively.

The UV spectral data were obtained with the International Ultraviolet Explorer (IUE, Boggess 1978a,b; Kondo 1987) in two runs: November, 1990 and September, 1991. The images were obtained with three cameras: the *Small Wavelength Prime* (SWP, 1200 to 2000 Å); the *Large Wavelength Prime* (LWP, 2000 to 3200 Å) and the *Large Wavelength Redundant* (LWR, 2000 to 3200 Å). We have also used some images from the IUE data archive (see last column of Tables 3a and 3b). The images are unidimensional vectors with a sampling of 1 Å.

2.2.1. Obtaining the combined spectrum of each star

Each star has been observed, sometimes more than once, in each of the two wavelength ranges. The reductions were made using the RDAF and IUEIDL packages at the University of Wisconsin-Madison. The first procedure in the data reduction is to combine all the images of a star to one spectrum. Corrections for the time degradation of the camera sensibility (Bohlin & Grillmair 1988a,b) are made first. At the time this reduction was done only corrections up to 1988 were available, so to correct the data obtained after that time we had to use an extrapolation. Also the cameras do not have the same efficiencies, so there may be a discontinuity in the overlap region between two spectra. It is generally assumed that the two spectra must have the same flux in the overlap region. As we are interested only in the ratio between spectra of the program and the comparison stars (see eq. 1) we have not corrected for this effect. The combined spectra did not present any discontinuities.

2.2.2. Determination of the extinction curves

We have obtained the extinction curves using the pair-method (Fitzpatrick & Massa 1986) which consists in comparing two stars of the same spectral type, but with different reddening. The assumption is that the program and comparison stars have exactly the same intrinsic spectra, the observed difference being due to the foreground interstellar medium. We estimated the error in this assumption by using different comparison stars.

From the B and V magnitudes and the fluxes, ϕ_i, the normalized extinction is given by:

$$\frac{E(\lambda - V)}{E(B - V)} = \frac{2.5\log(\frac{\phi_c}{\phi_r}) - V_r + V_c}{(B - V)_r - (B - V)_c} \tag{1}$$

where the subscripts r and c mean *reddened* and *comparison star*, respectively. Great care has been exercised in selecting appropriate comparison stars, specially for AZV 211 due to its relatively late spectral type. The comparison stars have been chosen from among SMC stars only, using the AZV82 catalog and excluding emission line stars, which are often variable and present anomalous color excesses due to circumstellar material. We also chose these unreddened stars within a spectral sub-class from AZV 211 with the purpose of matching as best we could this star's spectral type. Further, we chose to stay with comparison objects within about a magnitude of AZV 211. By using SMC stars, we also minimize the effect of metallicity differences between comparison stars and reddened stars, since two stars with the same optical spectral type but different metallicities may have different UV spectra. In addition, by using unreddened SMC objects the foreground

Galactic extinction is cancelled if it is homogeneous across the SMC angular field. We have later examined the UV lines to detect possible mismatches.

AZV 20 and AZV 211 have the same spectral type (A0 Ia), so we have used the same comparison stars, observed by us, for both of them (see Tables 3a and 3b). Stars of spectral type A0 Ia present some difficulties. The UV spectra change rapidly with spectral type so that a mismatch has a much greater effect than it does for stars of earlier type. Furthermore, since stars of this spectral type are cooler and their UV flux lower, it is more difficult to get a good signal-noise ratio. AZV 126 has a spectral type (B0Iw) very similar to that of AZV 398 (B2) and AZV 456 (B0-1), so there is an overlap in the comparison stars, taken from the IUE data archive, for all three (see Table 3b). The final list of comparison stars for each program star is: for AZV 20 and 211, the comparison stars were AZV 161, 270, 504 and SK 194; for AZV 126, the comparison stars were AZV 61, 317 and 454; for AZV 398 and AZV 456, the comparison stars were AZV 235, 242, 289, 317 and 488.

As noted above, the IUE spectra have 1 Å sampling. The extinction calculated with such a small wavelength step usually has a very poor signal-to-noise ratio. So we have also formed combined spectra with bins of 80 Å. The flux value in each 80 Å bin is assumed to be the sum of the fluxes in the 1 Å bins. The extinction curves are shown in Figs. 2 and 4. The curves with 1 Å bins (Fig. 2) are useful to identify spectral type mismatches and the noisier regions. The curves in the figures are the weighted average of the curves using different comparison stars and the error bars in the 80 Å curves (Fig. 4) are the average standard deviation. The weights used were the values of $\Delta(B-V)$, the difference between the program star and comparison star colors given in Table 3a and 3b. In this way we give greater weight to the reductions with the least reddened comparison stars.

For AZV 211 we initially determined extinction curves from the four comparison stars listed above. We found, however, that the curve using the comparison star AZV 161 was very different than the other three curves, and we suspect that this comparison star may be reddened. We have, therefore, excluded the curve using AZV 161 from the average curve for AZV 211 and for AZV 20. The resultant average curve for AZV 211 seems to follow the SMC standard with no bump and an enhanced FUV extinction (Figs. 2c and 4b).

AZV 20 has the noisest extinction curve (see Fig. 2a) in the sample despite the fact that it has a large color excess (see Table 3a) and we do not present for it a curve with 80 Å bins. The systematic increase in error with increasing frequency is due to the systematic decrease in signal-to-noise (see Fig. 2a). Where the extinction curve is less noisy, the values of the extinction are close to those for the typical SMC extinction curve (compare, for example, Fig. 2a to Fig. 2c and Fig. 2d at $\lambda^{-1} \approx 5.5\mu\mathrm{m}^{-1}$).

The extinction curves which we have redetermined for AZV 398 (Figs. 2d and 4c) and AZV 456 (Figs. 2e and 4d) are in perfect agreement with those of Prévot et al. (1984) and Lequeux et al. (1984), respectively.

The extinction for AZV 126 (Fig. 2b) will be discussed in section 4.1 below. AZV 215, for which we have obtained polarization data (Tables 1 and 4), has spectra available in the IUE data bank. It has however a very small $(B - V)$ value, comparable to possible comparison stars, so we could not determine a reliable extinction curve for it.

3. Qualitative study of optical polarization

3.1. Serkowski-law fits to the SMC Polarization Data

Serkowski (1973; see also Coyne et al. 1974) has shown that the Galactic interstellar polarization can be described by the following expression,

$$P(\lambda) = P_{max} \exp\left[-K \ln^2\left(\frac{\lambda_{max}}{\lambda}\right)\right] \quad (2)$$

where, from the observed P(λ) data, the parameters P_{max} , K and λ_{max} may be obtained.

P_{max}, the maximum polarization, depends on the column density of dust as well as the magnetic field structure and alignment efficiency along the line of sight. λ_{max} is the wavelength where P_{max} occurs and it is related to size of the dust particles (Coyne et al. 1974; Chini and Krügel 1983). K describes the width of the polarization curve.

In his original work Serkowski has taken K as a constant with a value of 1.15. Codina-Landaberry and Magalhães (1976) have shown that K varied for different lines of sight. Furthermore, from model fits they showed that K could be interpreted as being related to changes in the grain size along the line of sight. Wilking et al. (1980, 1982), using an extended wavelength range that included the IR, suggested a linear relation between K and λ_{max}. Whittet et al (1992), with a even larger sample, have provided the following relation:

$$K = (1.66 \pm 0.09)\lambda_{max} + (0.01 \pm 0.05)\ . \quad (3)$$

We have performed fits of the Serkowski relation to our SMC data in two ways: (1) allowing K to be a free parameter; and (2) using the above relation between K and λ_{max}. Admittedly, the first approach results in larger uncertainties for the derived parameters, especially K, but we felt that a first comparison between the K values from the SMC data and those from Galactic data would be of interest. Furthermore, a comparison between the two methods might help to judge the reliability of the derived parameters.

Table 4 gives the Serkowski fit parameters. In that table, column 8 gives the reduced χ^2 and column 9 gives the degree of freedom. The actual fits are shown in Fig. 1. The SMC polarization data can be well fit by the Serkowski relation by using either the 2- or 3-parameter method. The

3-parameter fits (solid lines in Fig. 1) are slightly better. This is especially true for AZV 215 and AZV 456. This point will be discussed further in sec. 5.

The values of λ_{max} from the two methods agree well within the errors. P_{max} from both fits shows an even closer agreement. Larger differences are found for the K parameter, although they may still be consistent within the large uncertainties. AZV 215 has data points at only 4 wavelengths and hence the uncertainties in K are particularly large. This is less so for AZV 456.

Table 4 shows that most of the SMC stars show λ_{max} smaller than the Galactic average, 0.55μm. In particular, this is true for two of the stars with the best polarimetric signal-to-noise, AZV 211 and AZV 398, which also have a typical SMC extinction curve (sec. 2.2.2). AZV 456, which has an UV bump (sec. 4.1), and AZV 215 show λ_{max} close to the Galactic norm. These results are in sharp contrast, for instance, with those for the LMC (Clayton and Martin 1985). For their sample of stars with measured extinction the smallest observed λ_{max} value is 0.52μm, with a median value of 0.58μm. Our results will be further discussed in sec. 5.

3.2. Polarization and Visible Extinction

The maximum polarization towards a given line-of-sight is related to the available amount of dust and depends on factors such as the magnetic field direction, grain alignment efficiency and the polarizing efficiency of the grains. Empirically, it is verified that for the Galaxy (Serkowski, Mathewson and Ford 1975)

$$P_{max} \leq 9.0E(B-V)\ . \tag{4}$$

A plot of P_{max} versus $E(B-V)$ for our sample is given in Fig. 3. We have used P_{max} values from Table 4. We have obtained the total color excesses as described in sec. 2.1.2 (Table 3a). When both our estimates and observed values were available (AZV 215, 398 and 456, Bouchet et al. 1985), we used the latter. For our $E(B-V)$ estimates, we used the ones derived with the spectral type-color relation by Brunet (1975). We have then corrected all color excesses by 0.05^{mag} to take into account the Galactic foreground reddening (sec. 2.1.2; Bessel 1991). The above empirical relation between P_{max} and color excess for the Galaxy is also plotted in Fig. 3. It is seen that the SMC stars also obey the Galactic relation between P_{max} and $E(B-V)$.

A related quantity of interest is the average ratio $P_{max}/E(B-V)$ for the SMC objects. This is 7.2 $\% mag^{-1}$ (from Tables 3a and 4). This value is comparable to the corresponding values for the Galaxy (5.0 $\% mag^{-1}$; Serkowski et al. 1975) and the LMC (6.0 $\% mag^{-1}$; Clayton and Martin 1985). Data from our survey in progress should be able to improve the estimate of this ratio for the SMC in the near future.

Serkowski et al. (1975) found a relationship between λ_{max} and R, R = 5.5 λ_{max}, for stars along several lines of sight. Whittet and van Breda (1978), with the aid of infrared photometry, confirmed that relation and obtained R = $(5.6\pm0.3)\lambda_{max}$. This correlation was re-examined and again confirmed by Clayton and Mathis (1988) using sight lines which included dense clouds as well as the more diffuse ISM. Using the data for AZV 211, 221 and 398, we obtain $\langle\lambda_{max}\rangle=(0.40\pm0.02)\mu$m. Bouchet et al. (1985) obtained from visual and near IR photometry for stars in the SMC a value of R = 2.72 ± 0.21, from which we obtain R/λ_{max} = (6.8 ± 0.6), still consistent with the Galactic relation. In other words, the somewhat smaller value of R for the SMC does translate into smaller values of λ_{max} in this galaxy. More data are clearly needed to examine this relation further.

4. Parametric study of UV extinction

4.1. Parametrization

In order to analyse objectively the extinction curves for the SMC we have for the first time fit them by using the parametrization of Fitzpatrick & Massa (1986). However, we have fit the parameters simultaneously, contrary to the approach of Fitzpatrick & Massa (1990). We have done this by minimizing the chi-square. The parametrization of Fitzpatrick & Massa (1990) is expressed by

$$\frac{E(x-V)}{E(B-V)} = c_1 + c_2 x + c_3 D(x;\gamma,x_o) + c_4 F(x) \ , \tag{5}$$

where

$$x = \lambda^{-1} \ ,$$
$$D(x;\gamma,x_o) = \frac{x^2}{(x^2-x_o^2)^2 + x^2\gamma^2}$$

and

$$F(x) = \begin{cases} 0.5392(x-5.9)^2 + 0.05644(x-5.9)^3, & if\ x \geq 5.9\mu\mathrm{m}^{-1}; \\ 0.0\ , & if\ x < 5.9\mu\mathrm{m}^{-1}. \end{cases}$$

We have not considered the star AZV 20 because of its very small signal-noise extinction curve (see Fig. 2a and discussion in sec. 2.2.2). We have performed the fits using the extinction curves with bins of both 1 Å (5 Å in the case of AZV 126) and of 80 Å to check the dependency of the parameters on the bin size. The results are presented in this order in Table 5 and in Fig. 4 together with the results from the fit of the Galactic curve (Seaton 1979).

We now discuss the fits for each star with reference to Table 5 and according to the three parts of equation 5: the linear part, the Drude function fit to the bump $D(x;\gamma,x_o)$, and the exponential fit to the increasing extinction into the FUV.

AZV 211 and AZV 398 both show the typical SMC extinction (Prévot et al. 1984) with no bump and a rapid increase in the UV and FUV extinction (Table 5, col. 8). Although these stars do not present the bump, any oscillation in the extinction curve might be interpreted artificially by the code as a small bump (see Table 5, cols. 10-13 and Fig. 4). For that reason, we have also performed the fits without the Drude function component. There was however no significant difference in the resultant parameters.

The extinction curve of AZV 456 is very similar to that for the Galaxy (Fig. 4; Lequeux et al. 1984) and, in fact, its extinction curve has been often referred to as a 'Galactic-type' curve. However, our fits show that its bump is shifted to the blue ($x_o = [4.67{\pm}0.03]\mu\mathrm{m}^{-1}$, Table 5) with respect to the Galactic average ($x_o = [4.596{\pm}0.019]\mu\mathrm{m}^{-1}$). For comparison, the largest value of x_o in the sample of Fitzpatrick & Massa (1986) is $4.63\mu\mathrm{m}^{-1}$. The width and intensity of the bump for AZV 456 are within the range of those for the Galaxy. In contrast, the three sight lines which show $x_o > 4.65\mu\mathrm{m}^{-1}$, seen through dense material, all appear to be associated with broad bumps (Cardelli & Savage 1988; Cardelli & Clayton 1991; Mathis 1994).

¿From studies of several Galactic sight lines, which included diffuse, dark cloud and star formation regions, Cardelli, Clayton and Mathis (1989) have shown that there is an average extinction law over the wavelength range 3.5μm to 0.125μm which is applicable to such environments. This mean extinction law, $A(\lambda)/A(V)$, depends only on the parameter R. They have noted, however, that a few sight lines, which included ones with broad bumps and those towards the LMC, did not conform to such a law. In Fig. 5, we plot the UV extinction curve of AZV 456 with the analytical law of Cardelli et al. (1989) for the values of $R = 2.73, 3.1$. It can be seen that the observed and analytical curves are discrepant, specially around the bump region, meaning that the line of sight to AZV 456 does not conform to the single parameter interpolation that performs well for the Galactic environs. Of course, the more typical, bumpless SMC extinction curves as presented by AZV 211 and AZV 398 do not obey the analytical expression for the Galaxy.

Among stars in our Galaxy which also present non-standard UV bumps, HD62542 has the most extreme bump, centered at $4.74\mu\mathrm{m}^{-1}$ (Cardelli and Savage 1988). Interestingly enough, the FUV extincion of HD62542 is actually closer to the SMC one. However, its bump is extremely shallow and its intensity is quite different (lower) compared to the Galactic average and AZV 456. In addition, our multicolor polarimetry of HD62542 (reported by Clayton et al. 1992) shows that its λ_{max} value is 0.59μm , quite different from the low λ_{max} values for the SMC (Table 4). This stresses the value of linear polarimetry in providing additional, independent information about the grains. In fact, in Paper II it will become clear that detailed simultaneous fitting of both extinction and polarization is more restrictive on the grain model parameters.

The parametrization of the extinction curve for AZV 126 with 1 Å bins converged to values which were not compatible with the observed curve. This may be due to the available signal-to-noise or some spurious effect in the extinction curve that the parametrization fit tried to include. We have hence fit eq. 5 to an extinction curve binned to 5 Å for AZV 126. This allowed a somewhat more reasonable parametrization. It nevertheless shows an abnormally small slope for the linear part (Table 5, col. 4). The Drude function fits (Table 5, cols. 10-13) indicate that it may have the extinction bump but shifted to the blue (Table 5, col. 11) with regards to both the Galaxy and AZV 456. It is also abnormally wide (Table 5, col. 10), although its intensity is within the Galactic range. The rise into the UV and FUV (Table 5, col. 8) is intermediate between that typical for the SMC and that for the Galaxy. The extinction curve for AZV 126 has a large intrinsic uncertainty and it must be viewed with caution.

4.2. Correlations between extinction components

Although the small number of extinction curves available for the SMC makes any search for correlations between the parameters difficult, there are tentative indications of correlations between the linear coefficients (c_1, c_2) and the coefficient (c_4) of the linear and FUV portions, respectively, of the extinction curves. These are shown in Fig. 6. The point with large error bars in that figure corresponds to parameters for the Galactic curve given in Table 5. The large errors are due to the fact that relatively few data points were available for the fit to the Galactic curve.

Figure 6 shows that the FUV curvature for the SMC, c_4, is correlated with the linear component in the sense that the higher the FUV curvature, the smaller the constant component, c_1 and the higher the slope of the linear component, c_2. In fact, the parameters c_1 and c_2 are perfectly correlated (Fitzpatrick & Massa 1988; Jenniskens & Greenberg 1993) and c_1 is not an independent parameter. If the FUV curvature does increase at the same time as the contribution of the linear component to the extinction, this can be interpreted as the result of a simultaneous decrease in the average size of the grains responsible for these various parts of the extinction curve. For the Galaxy no correlation is found between the linear rise and the extinction in the FUV (Jenniskens & Greenberg 1993). This may be a further indication of the differences between the ISM in the SMC and the Galaxy, where the correlation found may simply signify the increasingly larger number of smaller particles as we go from the Galaxy to the SMC.

The fact that AZV 211 and AZV 398 show a sizeable contribution to the FUV term in their extinction curves, quite larger than that of AZV 456, would appear to confirm that no positive correlation exists between the bump and the FUV curvature (Greenberg and Chlewicki 1983; Jenniskens & Greenberg 1993). In the Galaxy, the linear rise part (c_1, c_2) of the extinction curve is systematically less in dense media (Cardelli et al. 1989; Jenniskens & Greenberg 1993). The behaviour of the extinction curve for AZV 456 seems to follow the same trend. In contrast, the Galactic object HD204827 shows a steep FUV rise (Fitzpatrick & Massa 1990) while at the same time showing small λ_{max} (Whittet et al. 1992; Clayton et al. 1995), in line with the typical SMC sight lines. In the following section, we will return to this discussion.

5. Discussion

We now wish to discuss the data presented on the sample of stars in the SMC for which we have available both extinction curves and/or wavelength dependent polarization data.

Our extinction data suggest a correlation between the FUV curvature and the linear portion of the extinction curve (sec. 4.2). The stars for which the FUV contribution is more important, AZV 211 and AZV 398, do not show the bump, so the FUV curvature cannot be attributed to the same grains producing the bump. Further, these two stars show λ_{max} smaller than the Galactic average. Other SMC stars also present small λ_{max} values (Table 4, col. 2). Of the two stars in the SMC which have larger λ_{max} values, similar to those for the Galaxy, the one with the best signal-to-noise, AZV 456, has an extinction curve well determined (Prévot et al. 1984; sec. 4.1). This star does show the bump and is hence also characterized by grains larger than those found for the other lines-of-sight in the SMC. It may also be of interest to note that the bump in our Galaxy is not polarized (Clayton et al. 1992), so that the grains producing the bump are either spherical or not aligned.

It is tempting to conclude that the bump in the SMC would be present only along lines of sight characterized by large λ_{max}. This conclusion might be tenuous, since stars with both polarization and extinction curves reliably determined are very few in the SMC and there is only one known line of sight which shows the bump. However, we find it rather remarkable that AZV 456 has a Galactic gas-to-dust ratio (Bouchet et al. 1985, Fitzpatrick 1985b), an extinction curve similar to the Galaxy (Prévot et al. 1984; sec. 4.1) and a λ_{max} value similar to the Galactic average (sec. 3.1). All of the remaining stars in the sample of about 20 stars of Bouchet et al. (1985) and Fitzpatrick (1985b) show a gas-to-dust ratio roughly 10 times the Galactic average. The 3 stars in the sample of Prévot et al. (1984), which have this high gas-to-dust ratio, do not show the bump. In addition, in our sample of stars those which do not show the bump show small λ_{max} values. Extending the arguments of Fitzpatrick (1989) to include polarization data, we may say that, if the high gas-to-dust ratios are produced by conditions which also give rise to the typical SMC extinction law and small λ_{max} values, then our polarization measurements, as well as the extinction law of Prévot et al., may indeed represent the typical extinction and polarization properties of the dust in the SMC.

These results from our polarization data are important in order to improve the constraints on dust models for the SMC and as a test for inferences based solely on extinction data. Bouchet et al. (1985) point out that the value of R they have determined for the SMC, slightly smaller than the Galactic value, might suggest that the graphite grains would play a smaller role in the visible/IR. According to them, the size distribution of silicate grains, in the context of the MRN model (Mathis, Rumpl and Nordsieck 1977), would then have to be shifted towards larger grains. Our results that λ_{max} is in general smaller than in the Galaxy shows that the opposite is actually true.

The fact that the Serkowski fit to the 'normal λ_{max}' polarization curve of AZV 456 is significantly poorer when we use the Galactic relation between K and λ_{max} (sec. 3.1) may suggest that there is a different relationship between these parameters in the SMC. This suggestion is somewhat strengthened by a plot of the K vs. λ_{max} taken from the three parameter fits in Table 4 and shown in Fig. 7. While the K-λ_{max} relation for the SMC is similar to the Galactic one, a steeper slope is suggested. More data beyond the optical domain and for more stars are needed to clarify this.

AZV 456 and, to a certain degree, AZV 215 show λ_{max} values close to the Galactic norm. Their 3-parameter fits (Table 4 and Fig. 1) indicate that their polarization curves are narrower than the others. Regardless of the large uncertainties in K, Paper II will show that such narrow polarization curves are indeed more difficult to fit with dust models. The other stars (Table 4) are characterized by λ_{max} values smaller than 0.55μm.

These results can be interpreted in terms of the dust grain sizes. Values of λ_{max} close to 0.55μm indicate that the grains towards AZV 456 have average sizes close to those in the Galactic diffuse ISM, albeit possibly with a narrower size distribution. The line of sight to AZV 456 has an extended IR source (Schwering and Israel 1989) and it might indeed not represent the typical line of sight through the diffuse ISM in the SMC, as discussed above.

The lines of sight with smaller λ_{max} would evidence smaller average grain sizes. They are associated with no bump in their UV extinction curves, that is, with the extinction law which is considered typical of the SMC (Prévot et al. 1984). The correlation between the FUV curvature and linear part of the extinction curve, suggested by the data (sec. 4.2), indicate smaller average grain sizes producing the typical SMC extinction. The smaller average grain sizes inferred from our polarization data strengthen this interpretation.

As outlined in the Introduction, the SMC is a valuable laboratory for studying several aspects of galactic evolution and a test bench for stellar and interstellar constituent models (Westerlund 1989, 1990). With this in mind, it is instructive to consider suggestions and models that have been proposed for interstellar dust and how they fare in the SMC context, in addition to what has been already discussed in secs. 3 and 4.

Jenniskens, Ehrefreund & Désert (1992) have found a correlation between the amount of FUV rise (c_4, sec. 4.1) and the CH abundance in the line of sight to several Galactic stars. Since CH is directly proportional to molecular hydrogen, they suggested that the carrier of the FUV rise coexists with the medium containing H_2. They also suggested that the FUV rise is associated with Polycyclic Aromatic Hydrocarbons (PAHs). In the SMC, AZV 456 is related to an IR extended source (Schwering and Israel 1989) and its smaller gas-to-dust ratio suggests the presence of H_2 (Paper II). However, it is precisely AZV 456 which shows a small value of c_4 (Table 5 and Fig. 6). Our polarization data for AZV 456 shows that its line-of-sight has larger grains than the typical SMC line-of-sight and the fits we present in Paper II suggest the denser medium towards this object might result in the coagulation of smaller grains onto larger ones.

A related question concerns the PAH hypothesis and the IR emission of the SMC. Sauvage, Thuan and Vigroux (1990) presented the colors of the IRAS IR emission of the LMC and SMC and correlated them with the age and metalicity of the underlying stellar populations. Lequeux (1989) has nicely reviewed these and other IR data and their implications for the interstellar dust in the Magellanic Clouds. The integrated 12μm emission of the SMC (Rice et al. 1988, Schwering 1988) is specially low among irregular galaxies, suggesting that the PAHs, believed to be responsible for such emission, are less abundant, perhaps more destroyed by photodissociation by the more abundant FUV photons. This could be due to the interstellar radiation field (ISRF) in the SMC which is $\gtrsim 4$ times higher that of the Galaxy. The IRAS color-color diagrams suggest further that, besides the higher ISRF, the extreme properties of the SMC diagram are consistent with it being rich in small ($\lesssim 0.05\mu$m) grains responsible for the extinction shortwards of 2000Å. While the SMC extinction and (now) polarization data support the abundance of small grains, the steep FUV extincion and low 12μm emission simultaneously present in the SMC goes against the PAHs being responsible for the FUV rise as suggested by Désert, Boulanger & Puget (1990).

The higher ISRF in the SMC might also have a bearing on the absence of a UV bump in the SMC typical extinction curve. Leene and Cox (1987) found a correlation between the 60μm/100μm brightness ratio, a measure of dust temperature, and the height of the Galactic UV bump in the sense that the bump gets weaker when the 60μm/100μm ratio (and presumably the ISRF) gets higher. They suggested as a result that the particles responsible for the UV bump are very sensitive to the ISRF intensity. Jenniskens & Greenberg (1993) also found that the bump is sensitive to strong UV radiation fields from their studies of Galactic extinction curves and the environment. These results are consistent with the higher ISRF and general absence of the UV bump which characterize the SMC.

6. Summary

In order to study the grains in the SMC, which has an extinction curve very different from that for the Galaxy, we have obtained the first wavelength dependent polarization measurements for stars in the SMC. From an analysis of these and the extinction curves, for which we present some new IUE data, for a small sample of stars we reach the following conclusions: (1) the wavelength of maximum polarization, λ_{max}, determined from a fit of the Serkowski curve to the new polarization data, is generally smaller than in the Galaxy; (2) for AZV 456, the single well-studied case which shows the extinction bump at 2175 Å, λ_{max} is typical of that in the Galaxy; at the same time the bump for this star is shifted to the blue, as compared to the Galaxy, and its polarization curve is narrower; (3) the FUV curvature and linear component of the extinction curve increase simultaneously for stars with small λ_{max}.

We interpret our results to mean that the size distribution of grains is different in the SMC than it is in the Galaxy. In particular, the typical line-of-sight in the SMC is characterized by grains smaller than those in the Galaxy. This may be further evidence that the dust grains have formed somewhat differently and at a different rate in the SMC environment which has a gas-to-dust ratio ten times higher than that in the Galaxy. In Paper II we attempt to fit simultaneously both the extinction and polarization data for stars in the SMC by varying the mean size and the size distribution of the grains within the framework of classical models of grains.

This work has been supported by NASA Grant NAG 5 1463. It has been also partially supported by FAPESP (CVR: 89/3091-6; AMM: 89/1670-9, 92/3345-0 and 94/0033-3) and CNPq (AMM: 301558/79-5). AMM and CVR would like to acknowledge the hospitality provided by Dr. A. Code, Space Astronomy Laboratory and Astronomy Department, University of Wisconsin, where this research was partly done.

REFERENCES

Ardeberg, A., Brunet, J.P., Maurice, E. & Prévot, L. 1972, A&AS6, 249

Azzopardi, M. & Vigneax, J. 1982, A&AS50, 291 (AZV82)

Bessel, M.S. 1991, A&A242, L17

Boggess, A. et al. 1978a, Nature 275, 372

Boggess, A. et al. 1978b, Nature 275, 377

Bohlin, R.C. & Grillmair, C.J. 1988a, ApJS66, 209

Bohlin, R.C. & Grillmair, C.J. 1988b, ApJS68, 487

Bouchet, P., Lequeux, J., Maurice, E., Prévot, L. and Prévot-Burnichon, M.L. 1985, A&A149,330

Brunet, J. P. 1975, A&A43, 345

Burton, W.B., Deul, E.R., Walker, H.J. & Jongeneelen, A.A.W. 1986, in Light on Dark Matter, ed. F.P. Israel (Dordrecht: Reidel), 357

Cardelli, J.A. & Clayton, G.C. 1991, AJ101, 1021

Cardelli, J.A., Clayton, G.C. & Mathis, J.S. 1989, ApJ345, 245

Cardelli, J.A. & Savage, B.D. 1988, ApJ325, 864

Chini, R. & Krügel, E. 1983, A&A117, 289

Clarke, D. & Stewart, B.G. 1986, Vistas in Astronomy 29, 27

Clayton, G.C., Anderson, C.M., Magalhães, A.M., Code, A.D., Nordsiek, K.H., Meade, M.R., Wolff, M.J., Babler, B., Biorkman, K.S., Schulte-Ladbeck, R.E., Taylor, M. & Whitney, B.A. 1992, ApJ385, L53

Clayton, G.C., Green, J., Wolff, M., Zellner, N., Code, A.D. & Davidsen, A. 1996, ApJ, in press.

Clayton, G.C. & Martin, P.G. 1985, ApJ288, 558

Clayton, G.C., Martin, P.G. & Thomson, I. 1983, ApJ265, 194

Clayton, G.C. & Mathis, J.S. 1988, ApJ327, 911

Clayton, G.C., Wolff, M., Allen, R.G. & Lupie, O.L. 1995, ApJ445, 947

Codina-Landaberry, S. & Magalhães, A.M. 1976, A&A49, 407

Coyne, G.V., Gehrels, T. & Serkowski, K. 1974, AJ79, 581

Crampton, D. & Greasley, J. 1982, PASP94, 31

Désert, F.-X., Boulanger, F. & Puget, J.L. 1990, A&A237, 215

Fitzgerald, M.P. 1970, A&A4, 234

Fitzpatrick, E.L. 1985a, ApJ299, 219

Fitzpatrick, E.L. 1985b, ApJS59, 77

Fitzpatrick, E.L. 1986, AJ92, 1068

Fitzpatrick, E.L. & Massa, D., 1986, ApJ307, 286

Fitzpatrick, E.L. 1989, in IAU Symposium 135, Interstellar Dust, ed. L.J. Allamandola & A.G.G.M. Tielens (Dordrecht: Kluwer), 37

Fitzpatrick, E.L. & Massa, D. 1990, ApJS72, 163

Frecker, J. & Serkowski, K. 1976, Appl.Opt. 15, 605

Garmany, C.D., Conti, P.S. & Massey, P. 1987, AJ93, 1070

Greenberg, J.M. & Chlewicki, G. 1983, ApJ272, 563

Humphreys, R.M. 1983, ApJ265, 176

Jenniskens, P., Ehrefreund, P. & Désert, F.-X. 1992, A&A265, L1

Jenniskens, P. & Greenberg, J.M. 1993, A&A274, 439

Koorneef, J. 1982, A&A107, 247.

Koorneef, J. & Code, A.D. 1981, ApJ247, 860

Kondo, Y. 1987, Exploring the Universe with the IUE Satellite (Netherlands: Kluwer)

Leene, A. & Cox, P. 1987, A&A174, L1

Lequeux, J. 1989, in Recent Developments of Magellanic Cloud Research, ed. K.S. de Boer, F. Spite & G. Stasinska, (Paris: Obs. Paris), 119

Lequeux, J., Maurice, E., Prévot, L., Prévot-Burnichon, M. L. & Rocca-Volmerange B. 1984, A&A113, L5

Lequeux, J., Le Bourlot, J., Des Forets, G. P., Roueff, E., Boulanger & Rubio, M. 1994, A&A292, 371

Magalhães, A.M., Benedetti, E. & Roland, E.H. 1984, PASP96, 383

Magalhães, A.M., Loiseau, N., Rodrigues, C.V. & Piirola, V. 1990, in IAU Symposium 140, Galactic and Intergalactic Magnetic Fields, ed. R. Beck, P.P. Kronberg & R. Wielebinski (Dordrecth: Kluwer), 255

Magalhães, A.M., Rodrigues, C.V., Margoniner, V.E., Pereyra, A. & Heathcote, S. 1996, in Polarimetry of the Interstellar Medium, ed. D.C.B. Whittet & W. Roberge (San Francisco: ASP), in press.

Mathewson, D.S. & Ford, V.L. 1970 AJ75, 778

Mathis, J.S. 1994, ApJ422, 176

Mathis, J.S., Rumpl, W. & Nordsieck, K.H. 1977, ApJ217, 425

McNamara, D.H. & Feltz, K.H. 1980, PASP92, 587

Nandy, K., Morgan, D.H., Willis, A.J., Wilson, R., Gondhalekar, P.M. 1981, MNRAS196, 955

Prévot, M. L., Lequeux, J., Maurice, E., Prévot, L. & Rocca-Volmerange, B. 1984, A&A132, 389

Rice, W., Lonsdale, C.J., Soifer, B.T., Neugebauer, G., Kaplan, E.L., Lloyd, L.A., de Jong, T. & Habing, H.J. 1988, ApJS68, 91

Rodrigues, C.V. 1992, MSc Thesis, Instituto Astronômico e Geofísico, Universidade de São Paulo

Rodrigues, C.V., Magalhães, A.M. & Coyne, G.V. 1995, ApJ, submitted (Paper II)

Sanduleak, N. 1968 AJ73, 246

Sanduleak, N. 1969 AJ74, 877

Sauvage, M., Thuan, T.X. and Vigroux, L. 1990, A&A237, 296

Schmidt, Th. 1970, A&A6, 294

Schmidt, Th. 1976, A&AS24, 357

Schwering, P.B.W. 1988, Ph.D. Thesis, University of Leiden

Schwering, P.B.W. & Israel, F.P. 1989, A&AS79, 79

Seaton, M.J. 1979, MNRAS 187, 73p

Serkowski, K. 1973, IAU Symp. 52, Interstellar Dust and Related Topics, ed. J. M. Greenberg & H.C. van de Hulst (Dordrecth: Reidel), 145

Serkowski, K., Mathewson, D.S., & Ford, V.L. 1975, ApJ196, 261

Stahl, O., Buzzoni, B., Kraus, G., Schwarz, H., Metz, K., & Roth, M. 1986, The Messenger 46, 23

Wheeler, J. C., Sneden, C. & Truran Jr., J. W. 1989, ARA&A27, 279

Westerlund, B. E. 1989, in Recent Developments of Magellanic Cloud Research, ed. K.S. de Boer, F. Spite and G. Stasinska, (Obs. Paris: Paris), 159.

Westerlund, B. E. 1990, Astron. Astrophys. Rev. 2, 29

Whittet, D.C.B. and van Breda, I.G. 1978, A&A66, 57

Whittet, D.C.B., Martin, P., Hough, J. Rouse, M. Bailey, J. & Axon, D. 1992, ApJ386, 562

Wilking, B.A., Lebofsky, M.J., Martin, P.G., Rieke, G.H. & Kemp, J.C. 1980, ApJ235, 905

Wilking, B.A., Lebofsky, M.J. & Rieke, G. H. 1982, AJ87, 905

Xu, C. & Helou, G. 1994, ApJ426, 109

Table 1. SMC polarization data

Identification		Observed			Corrected			
AZV	SK	P	σ_P	θ_P	P	σ_P	θ_P	λ_{eff}
		(%)	(%)	(°)	(%)	(%)	(°)	(μm)
(1)	(2)	(3)	(4)	(5)	(6)	(7)	(8)	(9)
126	-	1.149	0.095	107.5	0.737	0.126	104.1	0.379
		1.175	0.055	109.3	0.725	0.105	106.6	0.439
		1.076	0.040	111.4	0.598	0.102	109.7	0.559
		0.781	0.078	110.1	0.325	0.129	105.3	0.664
		0.825	0.083	108.6	0.407	0.120	103.7	0.791
211	74	1.207	0.044	126.6	0.943	0.085	127.3	0.378
		1.243	0.027	124.8	0.955	0.083	125.0	0.438
		1.250	0.075	126.0	0.947	0.112	126.6	0.516
		1.175	0.017	126.1	0.873	0.085	126.8	0.559
		1.063	0.018	127.6	0.774	0.082	128.9	0.664
		0.986	0.042	131.1	0.728	0.085	133.7	0.790
		0.991	0.080	125.0	0.726	0.107	125.3	0.820
215	76	0.782	0.035	148.5	0.626	0.086	158.3	0.437
		0.907	0.032	148.6	0.741	0.089	157.4	0.557
		0.742	0.033	148.5	0.587	0.087	159.2	0.662
		0.653	0.060	148.7	0.512	0.095	160.0	0.791
221	77	1.125	0.099	138.3	0.903	0.129	148.4	0.377
		1.048	0.047	140.9	0.862	0.101	153.3	0.437
		1.014	0.042	141.5	0.838	0.103	155.2	0.558
		0.799	0.060	144.3	0.698	0.109	161.6	0.663
		0.659	0.084	143.0	0.557	0.119	162.5	0.791
398	-	2.114	0.108	131.4	1.856	0.130	132.5	0.380
		2.084	0.058	132.5	1.810	0.098	133.8	0.440
		2.038	0.042	131.9	1.751	0.093	133.2	0.560
		1.948	0.058	134.6	1.679	0.099	136.4	0.665
		1.464	0.072	134.8	1.218	0.103	137.0	0.791
456	143	0.959	0.074	163.9	0.842	0.086	167.0	0.376
		1.147	0.060	160.0	1.006	0.076	162.3	0.437

Table 1—Continued

Identification		Observed			Corrected			
AZV	SK	P (%)	σ_P (%)	θ_P (^{o})	P (%)	σ_P (%)	θ_P (^{o})	λ_{eff} (μm)
(1)	(2)	(3)	(4)	(5)	(6)	(7)	(8)	(9)
		1.323	0.172	156.7	1.156	0.179	158.4	0.516
		1.338	0.045	160.9	1.195	0.067	163.0	0.559
		1.259	0.050	160.7	1.120	0.069	162.9	0.671
		1.133	0.059	161.3	1.006	0.073	163.6	0.791
		0.950	0.089	163.2	0.830	0.099	166.2	0.820

Table 2. Foreground polarization corrections for various regions in the SMC

Region	P (%)	σ_P (%)	θ (deg)	σ_θ (deg)	N
I	0.47	0.09	113.6	14.0	6
II	0.30	0.08	124.1	8.0	10
III	0.17	0.05	145.0	8.2	11
IV	0.22	0.05	124.2	6.5	6
V	0.27	0.05	95.6	5.5	11

Table 3a. Relevant data on the reddened stars

Star	Sp	$(B-V)_0$[f]	V[g]	(B-V)	(U-B)	E(B-V)	IUE Images
AZV 20	*A0Ia*[a]	+0.02 -0.04	12.1	+0.29	-0.12	+0.27 +0.33	LWP 21313,14,15 SWP 42509, 39,40

AZV 126	*B0Iw*[b]	-0.24
		-0.25
			13.47	-0.02	-0.90	+0.22
						+0.23
							LWP 21279,80
							LWR 14947
							SWP 42506, 18908

AZV 211	*A0Ia*[d]	+0.02
		-0.04
			11.5	+0.10	-0.45	+0.08
						+0.14
							LWP 21279, 80
							LWR 14947
							SWP 42506, 18908

AZV 398	*B2*[e]	-0.17 -0.18	13.85	+0.09	-0.77	+0.26 +0.27 +0.37[h]	LWR 14963 SWP 18911
AZV 456	$B0-1$[e]	-0.24 -0.25	12.89	+0.10	-0.74	+0.34 +0.35 +0.36[h]	LWR 12347 SWP 16051

Table 3b. Relevant data on the comparison stars

Comparison Star	Reddened Star	Sp	$(B-V)_0$[f]	V	[g] (B-V)	(U-B)	IUE Images
AZV 61	AZV 126	$O5V$[c]	+0.01	13.68	-0.23	-0.98	LWP 19245
AZV 161	AZV 20 AZV 211	$A0I$[a]	+0.01	11.80	+0.03	-0.40	LWP 19245 SWP 40139
AZV 235	AZV 398 AZV 456	$B0Iw$[b]	-0.24	12.15	-0.12	-0.94	LWR 7239, 84 SWP 8293
AZV 242	AZV 398 AZV 456	$B1:I$[a]	-0.19	12.08	-0.10	-0.88	LWR 7242 SWP 8296
AZV 270	AZV 20 AZV 211	$A0Ia$[d]	+0.02	11.43	+0.03	-0.42	LWP 19241, 44 SWP 40134, 37
AZV 289	AZV 398 AZV 456	$B0.5I$[c]	-0.22	12.42	-0.14	-0.94	LWR 12345 SWP 16049, 18829
AZV 317	AZV 126 AZV 398 AZV 456	$B0Iw$[b]	-0.24	12.90	-0.20	-1.00	LWR 17264 SWP 10315, 22373
AZV 454	AZV 126	OV[e]	-	-	-0.19	-0.98	LWR 14948 SWP 18909, 22016
AZV 488	AZV 398 AZV 456	$B0Ia$[d]	-0.24	11.88	-0.13	-0.97	LWR 5642 SWP 6590
AZV 504	AZV 20 AZV 211	$B9Ia$[d]	-	11.91	-0.04	-0.46	LWP 19242 SWP 40138
SK 194	AZV 20 AZV 211	$B9Ia$[d]	-	11.74	+0.02	-0.53	LWP 21282, 83 SWP 42507, 08

[a]Humphreys (1983)

[b]Garmany et al. (1987)

[c]Crampton & Greasley (1982)

[d]Ardeberg et al. (1972)

[e]Prevot et al. (1984)

Table 4. Parameters of the Serkowski curve from fits of the SMC polarization data

Star	λ_{max} (μm)	$\sigma_{\lambda_{max}}$ (μm)	K	σ_K	P_{max} (%)	$\sigma_{P_{max}}$ (%)	χ^2	N
AZV 126	0.31	0.31	1.0	1.8	0.79	0.34	0.73	2
	0.20	0.99	0.3	1.6	0.8	1.4	0.77	3
AZV 211	0.37	0.22	0.48	0.67	0.956	0.089	0.11	4
	0.42	0.06	0.70	0.10	0.950	0.053	0.11	5
AZV 215	0.54	0.05	2.5	1.9	0.707	0.071	0.54	1
	0.48	0.12	0.81	0.20	0.666	0.061	0.66	2
AZV 221	0.42	0.12	1.2	1.3	0.892	0.073	0.09	2
	0.34	0.14	0.57	0.23	0.910	0.140	0.13	3
AZV 398	0.46	0.04	1.26	0.55	1.87	0.07	1.15	2
	0.40	0.05	0.68	0.08	1.86	0.08	1.17	3
AZV 456	0.57	0.02	2.06	0.53	1.19	0.05	0.30	4
	0.59	0.03	0.98	0.06	1.11	0.03	1.10	5

TABLE 5

PARAMETERS OF THE SMC EXTINCTION CURVES USING EXPRESSION OF FITZPATRICK & MASSA (1990)

Star (1)	c_1 (2)	σ_{c_1} (3)	c_2 (4)	σ_{c_2} (5)	c_3 (6)	σ_{c_3} (7)	c_4 (8)	σ_{c_4} (9)	γ (μm^{-1}) (10)	σ_γ (μm^{-1}) (11)	x_o (μm^{-1}) (12)	σ_{x_o} (μm^{-1}) (13)	A (μm^{-1}) (14)	χ^2 (15)	Bin (Å) (16)
AZV 126	-2.2	7.3	0.68	0.44	47	282	0.71	0.58	4.4	7.7	4.70	0.68	16.80	0.17	80
	-0.42	0.18	0.61	0.03	4.97	2.00	0.49	0.06	2.05	0.31	4.72	0.05	3.81	1.40	5
AZV 211	-8.6	2.8	3.09	0.52	0.17	0.95	1.1	1.6	0.5	1.3	4.24	0.27	-	0.06	80
	-8.53	0.20	3.03	0.04	0.46	0.20	1.24	0.18	0.79	0.15	4.16	0.03	-	0.75	1
	-7.70	1.70	2.96	0.37	-	-	1.10	1.60	-	-	-	-	-	0.11	80
	-7.90	0.13	2.97	0.03	-	-	1.08	0.17	-	-	-	-	-	0.80	1
AZV 398	-4.67	0.23	2.21	0.05	-0.01	0.03	1.00	0.27	0.13	0.35	4.26	0.08	-	1.03	80
	-4.63	0.02	2.18	0.01	0.01	0.01	1.05	0.02	0.095	0.09	4.60	0.01	-	5.80	1
	-4.57	0.16	2.22	0.04	-	-	1.00	0.02	-	-	-	-	-	2.54	80
	-4.73	0.02	2.23	0.01	-	-	0.95	0.02	-	-	-	-	-	7.80	1
AZV 456	-0.57	0.20	0.90	0.04	4.7	1.0	0.17	0.13	1.34	0.13	4.66	0.02	5.51	1.57	80
	-0.44	0.02	0.92	0.01	2.70	0.06	0.09	0.01	1.04	0.01	4.71	0.01	4.10	9.70	1
Seaton Curve	-0.4	2.0	0.75	0.31	4.0	4.4	0.22	0.54	1.05	0.55	4.59	0.12	5.98	0.02	-

Fig. 1.— Polarization for the SMC stars. Points with error bars represent our foreground corrected data. The solid lines and dashed lines show the 3- and 2-parameter Serkowski fits, respectively.

Fig. 2.— Extinction curves of SMC stars obtained using the pair-method and combined spectra with 1 Å sampling, except for AZV 126 (5 Å): (a) AZV 20; (b) AZV 126; (c) AZV 211; (d) AZV 398; (e) AZV 456. The curves for AZV 398 and AZV 456 were derived using in part IUE images of these objects obtained by Prévot et al. (1984) and Lequeux et al. (1984).

Fig. 3.— Polarization vs. E(B-V). The continuous line represents the Galactic empirical relation. See text (sec. 3.2) for discussion.

Fig. 4.— Parametric fits, using the Fitzpatrick & Massa (1986) representation, to the extintion curves for: (a) AZV 126; (b) AZV 211; (c) AZV 398; (d) AZV 456; (e) the Galaxy, where the fits made to the extinction curve with a sampling of 1 Å (in (a) the binning is 5 Å) are superimposed on the points for the extinction curve with a binning of 80 Å. The respective curves are: dashed, the linear portion; dotted, the Drude function; dashed-dotted, the exponential function for the UV and FUV; solid, the combined fit. See eq. 5.

Fig. 5.— The UV extinction curve of AZV 456 with the analytical curves of Cardelli et al. (1989) for R=2.72 (solid line) and R=3.1 (dashed line) superimposed.

Fig. 6.— The coefficient, c_4, for the exponential UV and FUV parts of the extinction curve plotted against the coefficients, c_1 and c_2, for the linear part of the extinction curve. See eq. 5.

Fig. 7.— K versus λ_{max} for SMC stars (this work) from the 3-parameter fits. The solid line is the Galactic relationship (Whittet et al. 1992).

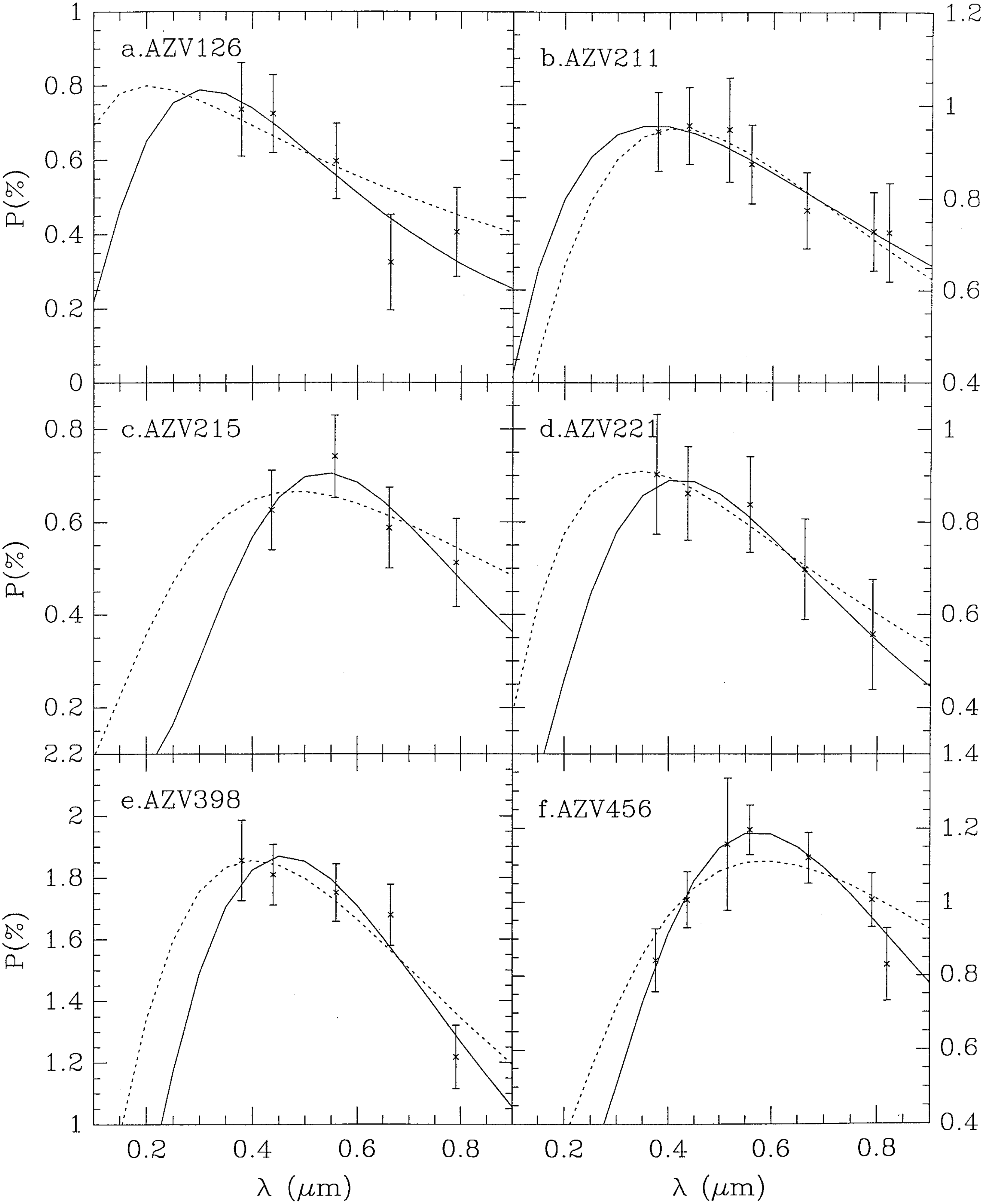
a.AZV126
b.AZV211
c.AZV215
d.AZV221
e.AZV398
f.AZV456
P(%)
λ (μm)
0.2
0.4
0.6
0.8
1
1.2
1.4
1.6
1.8
2
2.2

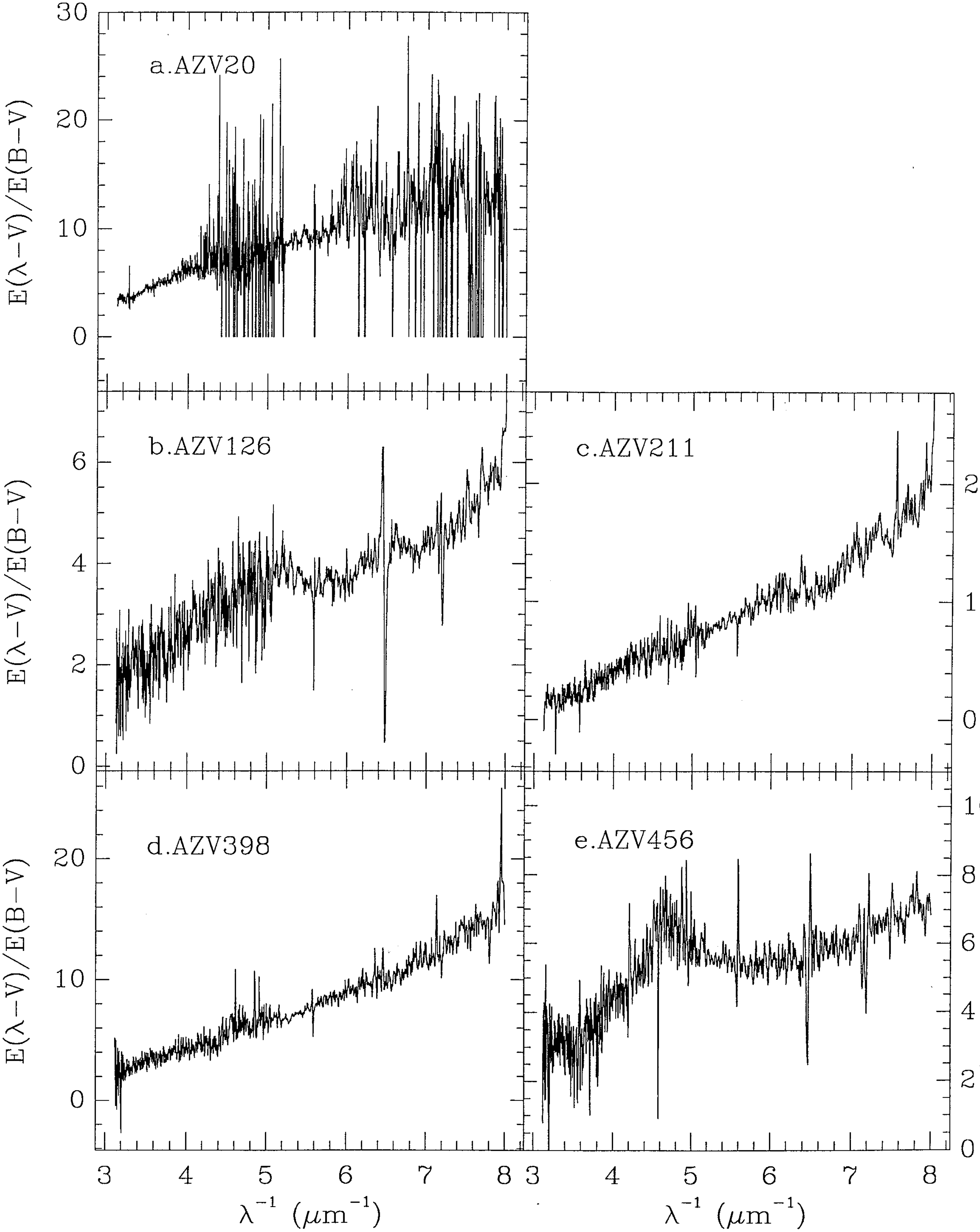
a.AZV20
b.AZV126
c.AZV211
d.AZV398
e.AZV456
E(λ−V)/E(B−V)
λ⁻¹ (μm⁻¹)

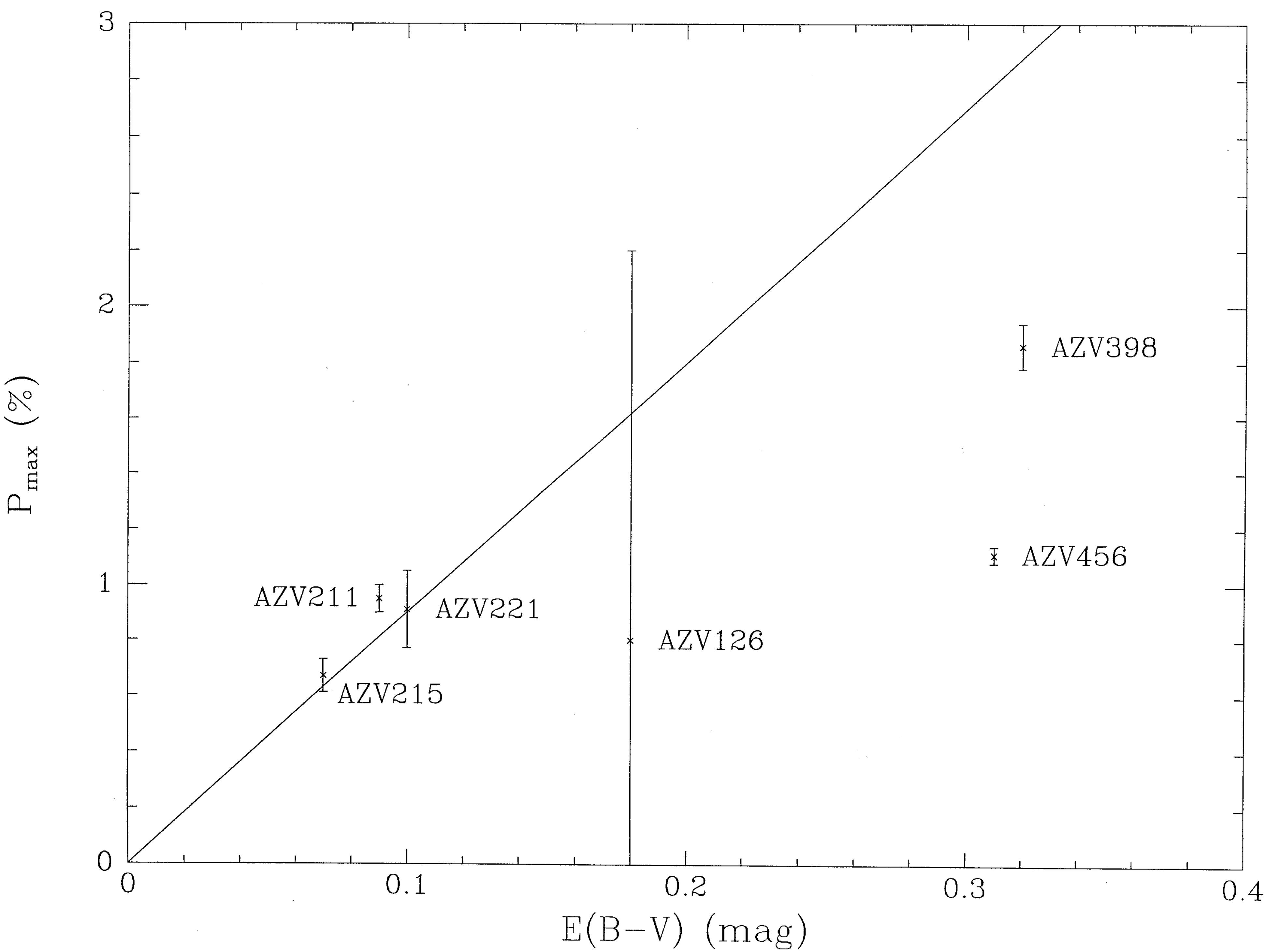

AZV398
AZV456
AZV211
AZV221
AZV126
AZV215
P_{max} (%)
E(B−V) (mag)
0
1
2
3
0.1
0.2
0.3
0.4

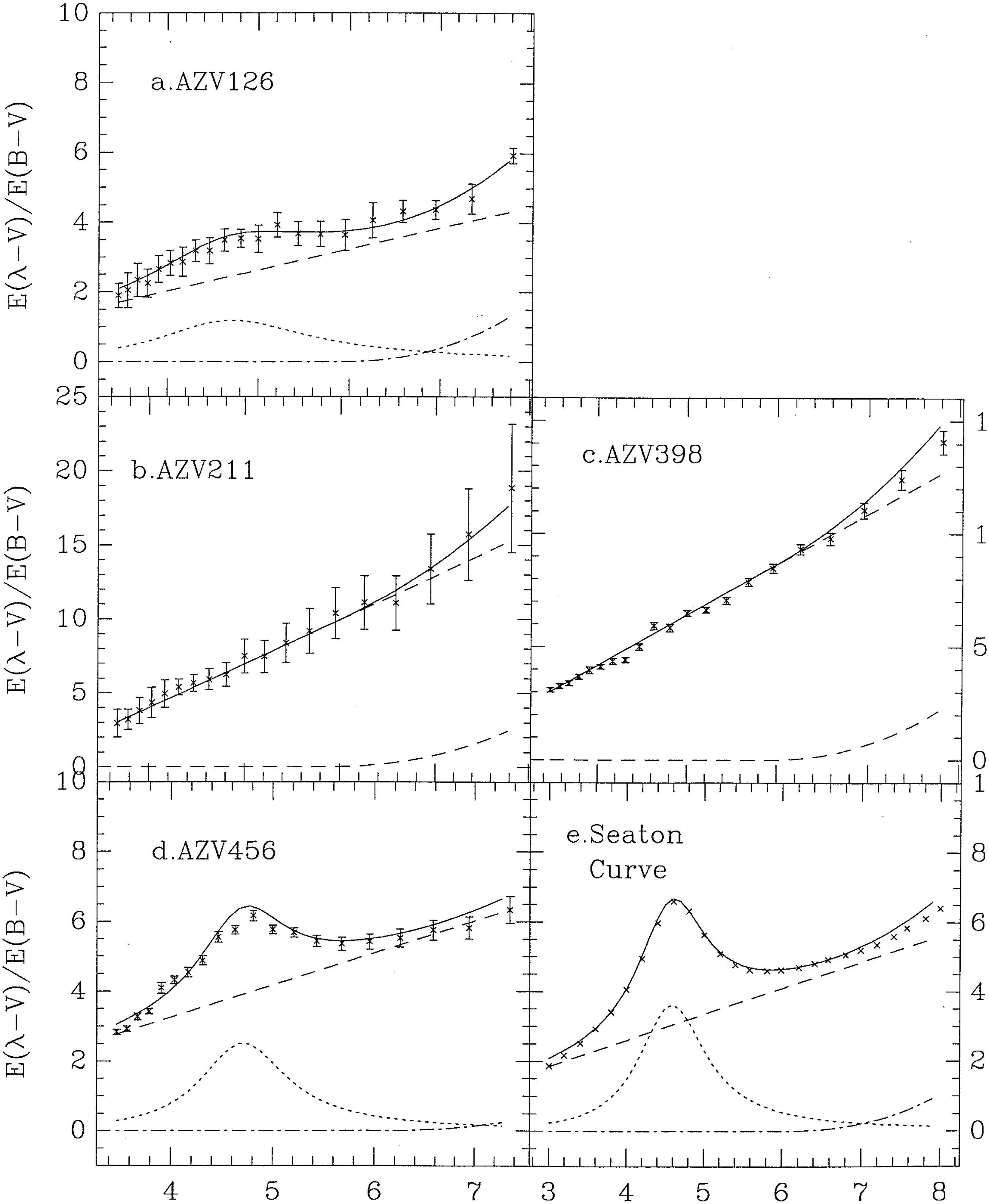
a.AZV126
b.AZV211
c.AZV398
d.AZV456
e.Seaton Curve
E(λ−V)/E(B−V)
λ^{-1} (μm^{-1})

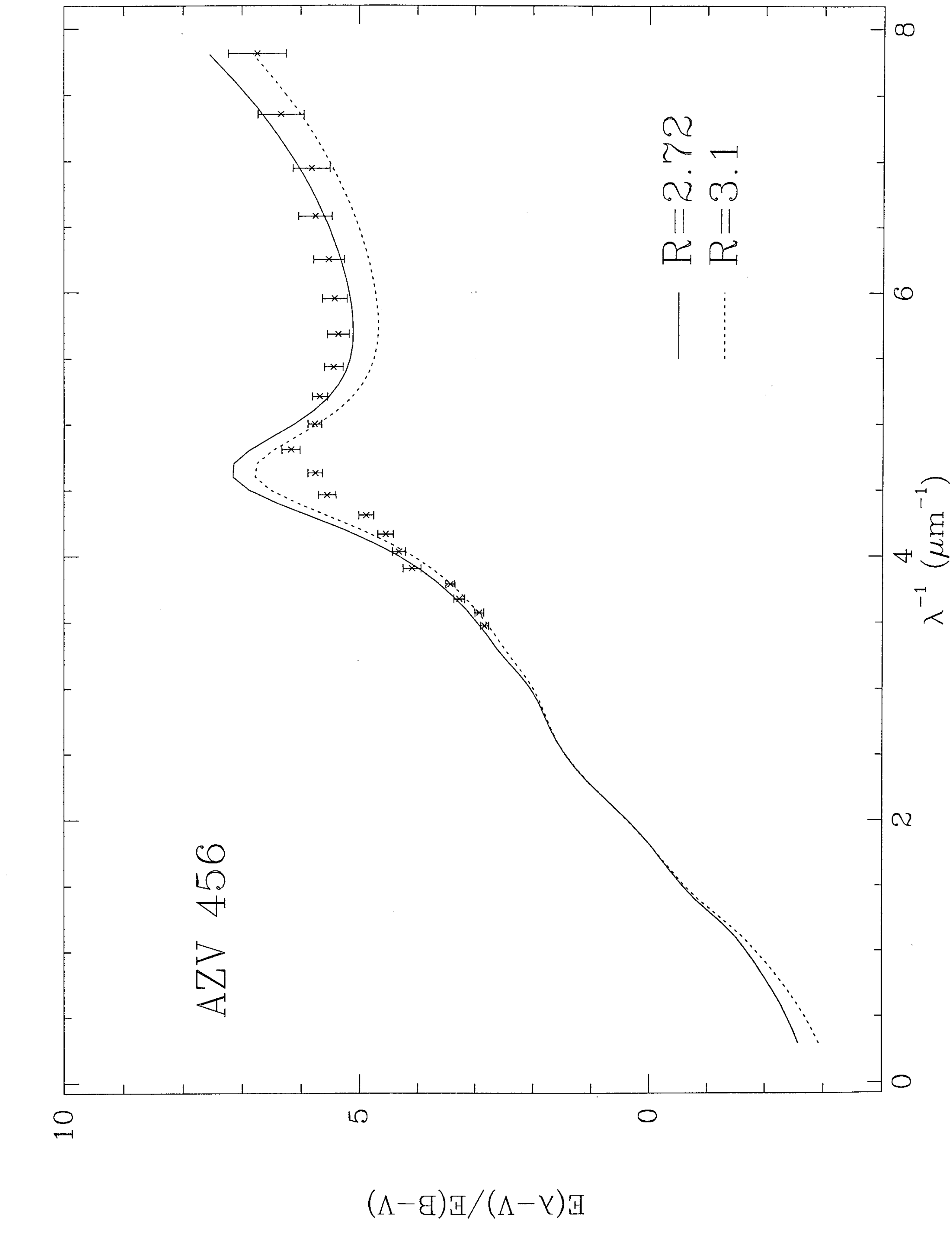
AZV 456
R=2.72
R=3.1
0
2
4
6
8
λ^{-1} (μm^{-1})
10
5
0
E(λ−V)/E(B−V)

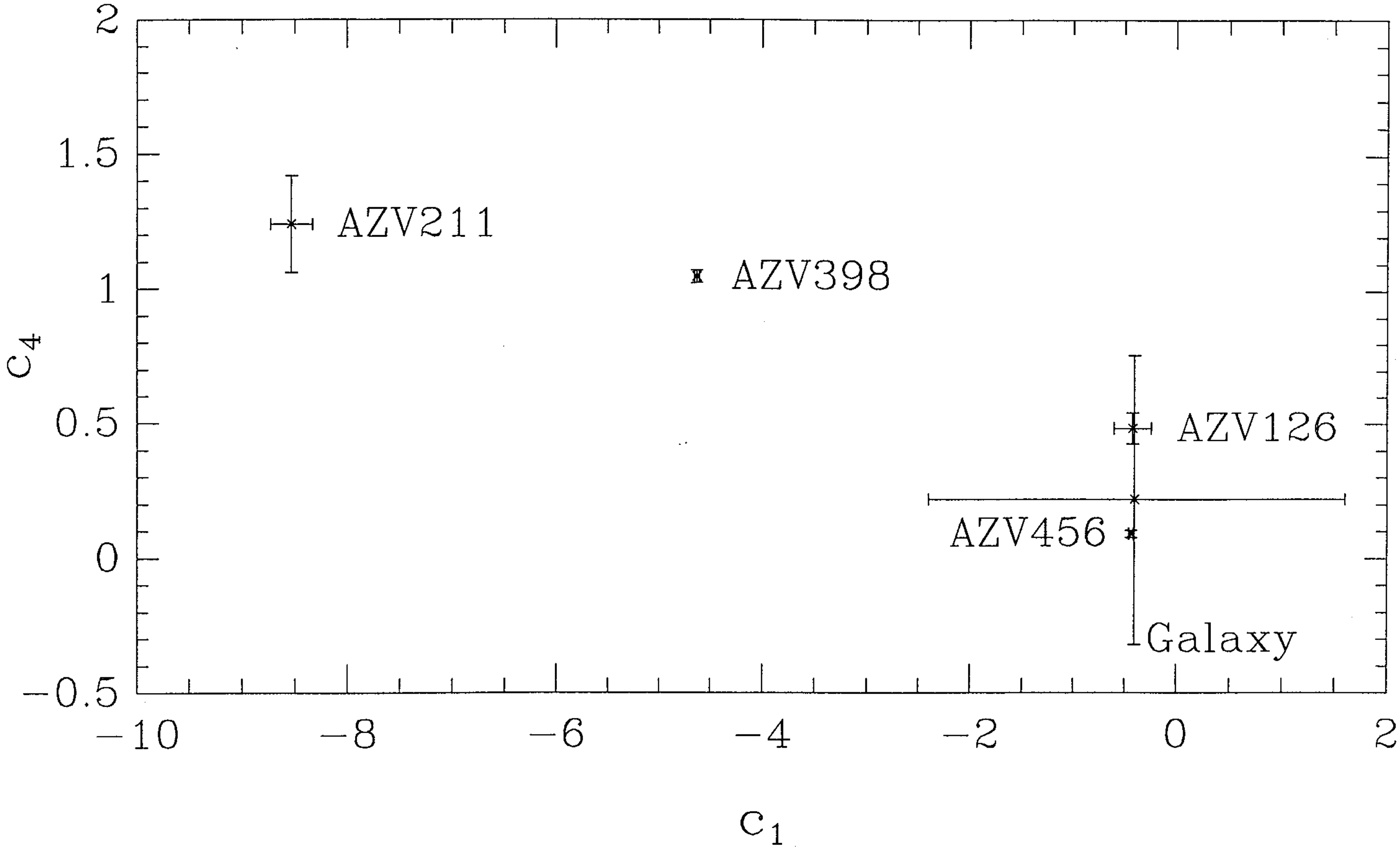
AZV211
AZV398
AZV126
AZV456
Galaxy
c_4
c_1
2
1.5
1
0.5
0
−0.5
−10
−8
−6
−4
−2
0
2

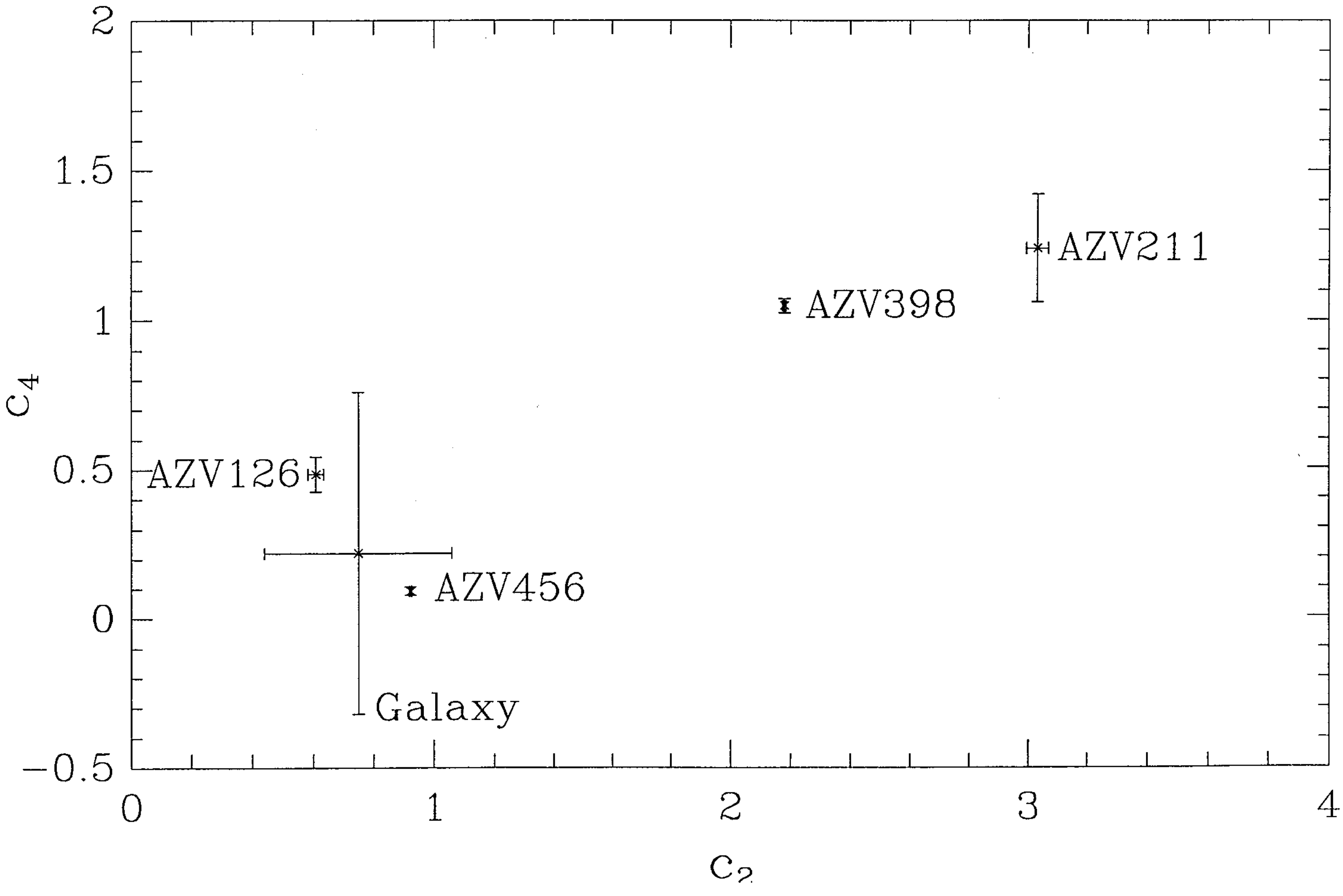
AZV211
AZV398
AZV126
AZV456
Galaxy
c_4
c_2
2
1.5
1
0.5
0
−0.5
0
1
2
3
4

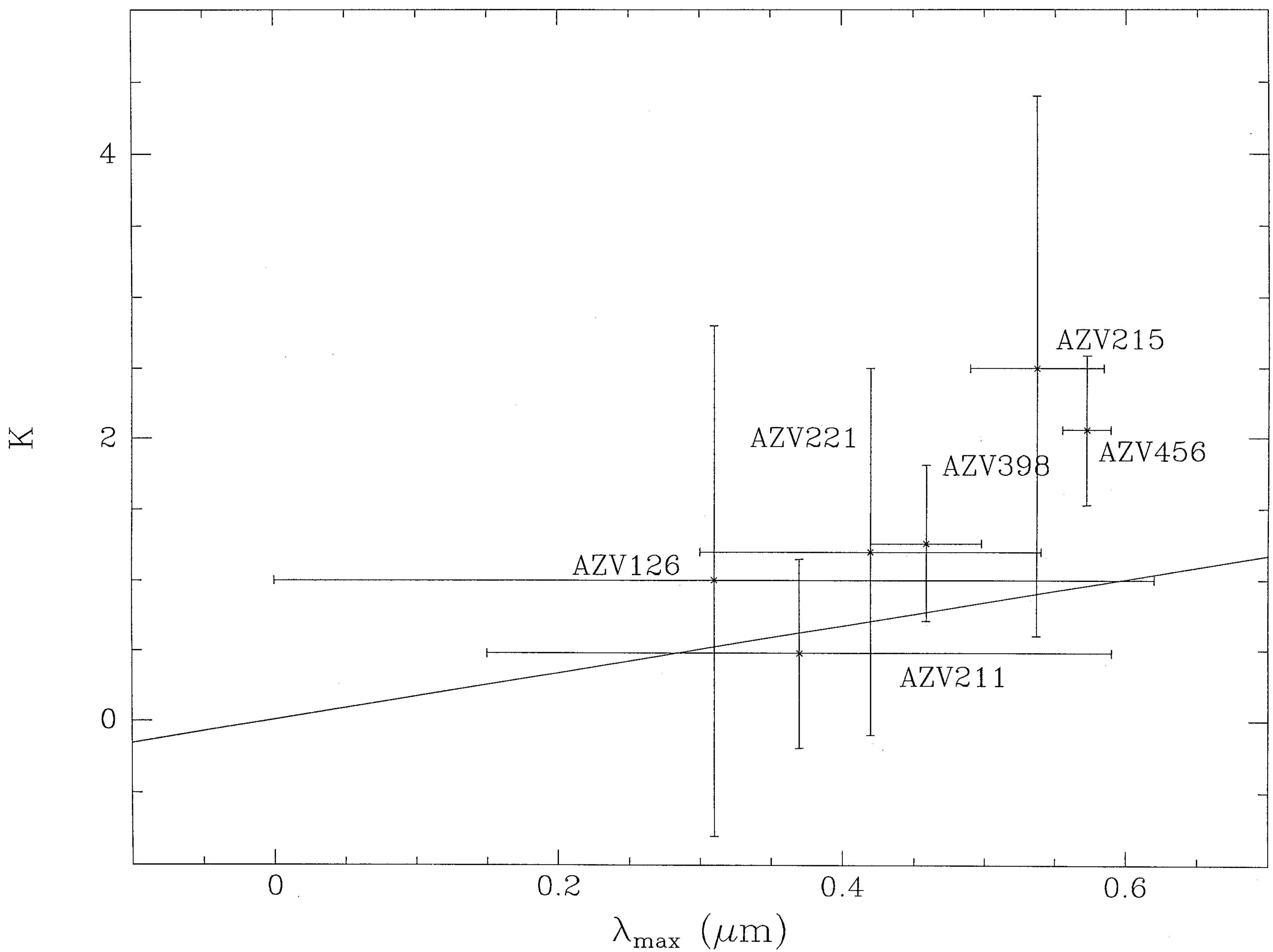
K
4
2
0
0
0.2
0.4
0.6
λ_{max} (μm)
AZV215
AZV221
AZV398
AZV456
AZV126
AZV211